HOMOTOPY PERTURBATION METHOD TO MHD NON-NEWTONIAN NANOFLUID FLOW THROUGH A POROUS MEDIUM IN ECCENTRIC ANNULI WITH PERISTALSIS

Mohamed Abou-zeid [a,b]

a) Department of Mathematics, Faculty of Education, Ain Shams University, Heliopolis, Cairo, Egypt

b) Department of Mathematics, Faculty of Science, University of Tabuk, Tabuk, Saudi Arabia

Abstract

In this contribution, the magnetohydrodynamic non-Newtonian nanofluid flow through a porous medium in eccentric annuli with peristalsis is investigated. This has been done under the combined effect of viscous dissipation and radiation. The inner annulus is rigid and at rest, while the outer annulus has a sinusoidal wave traveling down its wall. The fundamental equations are modulated under the long wave length assumptions, and a closed form of solution is obtained for the axial velocity. While, homotopy perturbation solution is obtained, which satisfies the energy and nanoparticles equations. Numerical results for the axial velocity, temperature and nanoparticles phenomena distributions as well as the reduced Nusselt number and Sherwood number are obtained and tabulated for various parametric conditions.

Key words: *Peristaltic flow; Non-Newtonian nanofluid; Porous medium; Heat transfer; Eccentric annuli.*

1. Introduction

Nanofluid is a liquid containing nanometer-sized particles (having diameter less than 100 nm), called nanoparticles. The nanoparticles are typically made up of metals, oxides, and carbides or carbon nanotubes. Nanofluids are produced by dispersing the nanometer-scale solid particles into base liquids with low thermal conductivity such as water, ethylene glycol (EG), oils, etc. [1]. The heat conduction has a great importance in many industrial heating or cooling equipments. Recently, there is a great advancement in the study of the flow of nanofluids with convective heat transfer [2]. Boundary layer flow of nanofluid in the region of stagnation point towards a stretching sheet has been addressed by Mustafa et al. [3]. Recently, many authors have investigated the nanofluid flow for different geometric surfaces, e.g., Ho et al. [4], Santra et al. [5], Mahmoudi et al. [6,7], Abu-Nada [8], Khalid and Vafai [9], Kuznetsov and Nield [10] and Choi [11].

* Author 's e-mail: master_math2003@yahoo.com

It may be noted that the particle size is an important physical parameter in nanofluids because it can be used to tailor the nanofluid thermal properties, as well as the suspension stability of nanoparticles. But, For the nano-scale thin liquid film flows, a fluid molecular layer attached to the wall molecules behaves as an extended wall layer, which induces increased shearing in the middle of the fluid. Researchers in nanofluids have been trying to exploit the unique properties of nanoparticles to develop stable as well as highly conducting heat transfer fluids. Nanofluids have many applications such as transportation, electronics cooling, defense, space, nuclear systems cooling, nuclear systems cooling, heat exchanger, and biomedicine. In view of its mechanical properties, silk cocoon is an "emperor's new clothes" for pupa. A theoretical analysis is given to explain the fascinating phenomenon by a fractal nano-hydrodynamic model for discontinuous membrane composed of hierarchical silk cascade. It is found that the nano-cocoon mechanism could help the further design of bio-mimetic artificial clothes for special applications [12].

It is now a well-accepted fact that many physiological fluids behave in general like suspensions of deformable or rigid particles in a Newtonian fluid. Blood, for example, is of red cells, white cells and platelets in plasma. Another example is cervical mucus, which is a suspension of macromolecules in a water-like liquid. In view of this, some researchers have tried to account for the suspension behavior of biofluids by considering them non-Newtonian [13]. The peristaltic flow of non-Newtonian fluid has attracted the attention of many researchers in the past three decades, mainly because of its relevance to biological systems and industrial applications. A mathematical model of peristaltic motion of nanofluid in a channel with compliant walls is presented by Mustafa et al. [14]. They have computed numerical and analytic solutions of the developed differential system which are found in excellent agreement. Akbar et al. [15, 16] studied the effects of endoscope on the peristaltic transport of nanofluids and the slip effects on the peristaltic transport of nanofluid in an asymmetric channel. The problem of the unsteady peristaltic mechanism with heat and mass transfer of an incompressible micropolar non-Newtonian fluid in a two-dimensional channel is analyzed by Eldabe and Abou-zeid [17]. They include the viscoelastic wall properties, all micropolar fluid parameters as well as the viscous dissipation effect. Recently, a vast amount of literature is available on peristaltic flow of Newtonian and non-Newtonian nanofluid [18-21].

The pipe eccentricity effects are used to design or evaluate technological operations in oil fields. Nevertheless, a predominant role in drilling and cementing operations is played by pipe eccentricity [22]. Walton and Bittleston [23] obtained analytical and numerical solutions for Bingham plastic flow in a narrow eccentric annulus. Magnetohydrodynamic steady laminar flow and heat transfer of an incompressible, electrically conducting, non-Newtonian fluid in an eccentric annulus is studied by Ahmed and Attia [24]. Elsayed et al. [25] investigated the peristaltic flow and heat transfer of non-Newtonian fluid in an eccentric uniform annulus in the presence of external uniform magnetic field.

The present paper extends the work of Elsayed et al. [25] to include porous medium and nanofluid with different non-Newtonian fluid (biviscosity model). The following analysis include slip velocity boundary condition. The fundamental equations which govern this flow have been modeled under long-wavelength assumption and a closed form for the axial velocity is presented. Homotopy perturbation solutions for the energy and nanoparticles equations are obtained. Also, the reduced Nusselt number and Sherwood number at the outer annulus are obtained and tabulated for positive and negative eccentricity. The relation between the different parameters of motion is studied in order to investigate how to control the motion of the fluid by changing these parameters.

2. Mathematical formulation

The flow with heat transfer of an incompressible non-Newtonian nanofluid obeying biviscosity model through a porous medium in the gap between two eccentric uniform annulus is considered. The inner annulus is rigid and at rest, while the outer annulus has a sinusoidal wave traveling down its wall. A cylindrical coordinate system (r, ψ, z) is chosen for the annuli with r in the radial direction, z along the center line, the inner annulus is at $r = r_i$ and kept at a temperature T_i , while the outer annulus is at $r = r_o$ and kept at a temperature T_o , the equation for the outer surface is [25]:

$$R(r,\psi,z) = \sqrt{r_o^{\,2} - e^2 \sin^2 \psi} - e\cos\psi \,, \tag{1}$$

where $$r_o = R_o + b\cos\frac{2\pi}{\lambda}(z - c\,t)\,, \tag{2}$$

where e is the eccentricity, R_o signifies the radius of the outer annulus at inlet, b is the wave amplitude, λ is the wavelength, c is the wave velocity and t is the time.

The biviscosity model [13] can be written as

$$\tau_{ij}=\begin{cases}2\left(\mu_B+{p_y}\big/{\sqrt{2\pi}}\right)e_{ij}\,, & \pi\ge\pi_c\\ 2\left(\mu_B+{p_y}\big/{\sqrt{2\pi_c}}\right)e_{ij}\,, & \pi<\pi_c\end{cases}. \tag{3}$$

We introduce the following non-dimensional parameter $\beta=\mu_B\sqrt{2\pi_c}\,/\,p_y$,where p_y is the yielding stress, $\pi = e_{ij}\,e_{ij}$, where e_{ij} is the(i,j) component of the deformation rate and the value of β denotes the upper limit of apparent viscosity coefficient. For ordinary Newtonian fluid ($p_y=0$).

Since the flow parameters are independent of the azimuthal coordinate ψ, the velocity is given by $\underline{V}$ = (u, 0, w). A uniform magnetic field $\underline{B}$ = (0, B_0, 0) is applied in a transverse direction. The governing continuity, momentum, temperature, and nanoparticles equations are

$$\frac{\partial u}{\partial r}+\frac{u}{r}+\frac{\partial w}{\partial z}=0\,, \tag{4}$$

$$\rho_f\left(u\frac{\partial u}{\partial r}+w\frac{\partial u}{\partial z}\right)=-\frac{\partial P}{\partial r}+\mu_B\,(1+\beta^{-1})\left(\frac{\partial^2 u}{\partial r^2}+\frac{1}{r}\frac{\partial u}{\partial r}-\frac{u}{r^2}+\frac{\partial^2 u}{\partial z^2}\right)-\frac{\mu_B}{k_p}u\,, \tag{5}$$

$$\rho_f\left(u\frac{\partial w}{\partial r}+w\frac{\partial w}{\partial z}\right)=-\frac{\partial P}{\partial z}+\mu_B\,(1+\gamma^{-1})\left(\frac{\partial^2 w}{\partial r^2}+\frac{1}{r}\frac{\partial w}{\partial r}-\frac{\partial^2 w}{\partial z^2}\right)-\frac{\mu_B}{k_p}w-\sigma B_0^2 w\,, \tag{6}$$

$$\begin{aligned}(\rho c)_f\left(u\frac{\partial T}{\partial r}+w\frac{\partial T}{\partial z}\right)&=k\left(\frac{\partial^2 T}{\partial r^2}+\frac{1}{r}\frac{\partial T}{\partial r}+\frac{\partial^2 T}{\partial z^2}\right)-\frac{1}{r}\frac{\partial (rq_r)}{\partial r}+\mu_B\,(1+\beta^{-1})\left(\left(\frac{\partial u}{\partial r}\right)^2\right.\\&\left.+\left(\frac{\partial u}{\partial z}+\frac{\partial w}{\partial r}\right)^2+\left(\frac{\partial w}{\partial z}\right)^2\right)+(\rho c)_p\left[D_B\left(\frac{\partial T}{\partial r}\frac{\partial f}{\partial r}+\frac{\partial T}{\partial z}\frac{\partial f}{\partial z}\right)+\frac{D_T}{T_o}\left(\left(\frac{\partial T}{\partial r}\right)^2+\left(\frac{\partial T}{\partial z}\right)^2\right)\right],\end{aligned} \tag{7}$$

$$u\frac{\partial f}{\partial r}+w\frac{\partial f}{\partial z}=D_B\left(\frac{\partial^2 f}{\partial r^2}+\frac{1}{r}\frac{\partial f}{\partial r}+\frac{\partial^2 f}{\partial z^2}\right)+\frac{D_T}{T_o}\left(\frac{\partial^2 T}{\partial r^2}+\frac{1}{r}\frac{\partial T}{\partial r}+\frac{\partial^2 T}{\partial z^2}\right). \tag{8}$$

where u and w are the velocities in the r and z directions, respectively ρ_f and ρ_p are the density of the fluid and the particles respectively, P is the fluid pressure, k_p is the permeability of the porous medium, σ is the electrical conductivity of the fluid, T is the fluid temperature, k is the thermal conductivity of the fluid, $(\rho c)_f$ and $(\rho c)_p$ are heat capacity of the fluid and effective heat capacity of the nanoparticle material, q_r is the radiative heat flux, f is the nanoparticle phenomena, D_B is Brownian diffusion coefficient and D_T is the thermophoretic diffusion coefficient.

Non-Newtonian nanofluid has a slip velocity, which is expressed as [25]

$$w = -\gamma_v \, \lambda_m \left(\frac{\partial w}{\partial r} \right)\Bigg|_{r=R} , \tag{9}$$

where λ_m is the mean free path of the fluid molecules and γ_v depends on the interaction properties of fluid with the surface. The boundary conditions for this system are given by

$$\left.\begin{array}{l} u = 0 \;, \quad w = 0 \;, \quad T = T_i \;, \quad f = f_i \,, \quad at \quad r = r_i \\ u = \dfrac{\partial R}{\partial t} \;, \quad w = -\gamma_v \, \lambda_m \left(\dfrac{\partial w}{\partial r} \right)\Bigg|_{r=R} \;, \quad T = T_o \;, \quad f = f_o \quad at \quad r = R \end{array}\right\} . \tag{10}$$

The appropriate non-dimensional variables for the flow are defined as

$$\begin{array}{l} r^* = \dfrac{r}{L} \,, \; z^* = \dfrac{z}{\lambda} \,, \; u^* = \dfrac{\lambda}{c\,L} u \,, \; w^* = \dfrac{w}{c} , \; V_0{}^* = \dfrac{V_0}{c} , \; P^* = \dfrac{L^2}{\lambda\, c\, \mu_B} P \,, \; t^* = \dfrac{c}{\lambda} t, \\ \theta = \dfrac{T - T_o}{T_i - T_o} , \; f^* = \dfrac{f - f_o}{f_i - f_o} , \; \tau^* = \dfrac{R}{\mu\, c} \tau , \; r_i^* = \dfrac{r_i}{L} , \; r_o^* = \dfrac{r_o}{L} , \; \delta = \dfrac{L}{\lambda} \;, \; \varepsilon = \dfrac{e}{L} \,, \\ \phi = \dfrac{b}{L} , \; M = \dfrac{\sigma B_0^2 \, L^2}{\mu_B} , \; Da = \dfrac{k_p}{L^2} , \; \mathrm{Re} = \dfrac{c\,L}{\nu_B} , \; Ra = \dfrac{4\sigma^* T_1^3}{k\, k_R} , \; Ec = \dfrac{c^2}{c_P (T_i - T_o)} , \\ \mathrm{Pr} = \dfrac{\mu_B \, c_P}{k} , \; Br = Ec \, \mathrm{Pr} \,, \; N_t = \dfrac{D_T \,(T_i - T_o) (\rho c)_p}{T_o \,(\rho c)_f \; c\,L} , \; N_b = \dfrac{D_B \,(f_i - f_o) (\rho c)_p}{(\rho c)_f \; c\,L} \end{array} , \tag{11}$$

where L is the mean annular gap width, δ is the wave number, ε is the dimensionless, ϕ is amplitude ratio, Re is Reynolds number, M is the magnetic parameter, Da is Darcy number, Ra is the radiation parameter, Ec is Eckert number, Pr is Prandtl number , Br is Brinkman number, N_t is the thermophoresis parameter, and N_b is Brownian motion parameter.

Next, Rosseland approximation [26] is assumed, which leads to the radiative heat flux, q_r , given by

$$q_r = \frac{-4\sigma^*}{3k_R} \frac{\partial T^4}{\partial r} , \tag{12}$$

where σ^* is Stefan Boltzmann constant and k_R is the mean absorption coefficient. Assuming that the temperature differences are sufficiently small such that T^4 may be expressed as a linear function of temperature, then Taylor series for T^4 about T_o, after neglecting higher order terms, is given by [26]

$$T^4 \approx 4T_o^3\, T - 3T_o^4\,. \tag{13}$$

With the help of equation (11) and after dropping the star mark for simplicity, Eqs. (4)–(8) under the assumptions of long wavelength and low-Reynolds number approximation take the form

$$\frac{\partial u}{\partial r} + \frac{u}{r} + \frac{\partial w}{\partial z} = 0\,, \tag{14}$$

$$\frac{\partial P}{\partial r} = 0\,, \tag{15}$$

$$\frac{\partial P}{\partial z} = \left(1+\beta^{-1}\right)\left(\frac{\partial^2 w}{\partial r^2} + \frac{1}{r}\frac{\partial w}{\partial r}\right) - \left(\frac{1}{Da} + M\right) w\,, \tag{16}$$

$$\left(1+\frac{4}{3}Ra\right)\left(\frac{\partial^2 \theta}{\partial r^2} + \frac{1}{r}\frac{\partial \theta}{\partial r}\right) + \Pr Br\left(1+\beta^{-1}\right)\left(\frac{\partial w}{\partial r}\right)^2 + \Pr N_b\left(\frac{\partial \theta}{\partial r}\frac{\partial f}{\partial r}\right) + \Pr N_t\left(\frac{\partial \theta}{\partial r}\right)^2 = 0\,, \tag{17}$$

$$\frac{\partial^2 f}{\partial r^2} + \frac{1}{r}\frac{\partial f}{\partial r} + \frac{N_t}{N_b}\left(\frac{\partial^2 \theta}{\partial r^2} + \frac{1}{r}\frac{\partial \theta}{\partial r}\right) = 0\,. \tag{18}$$

Thus, the boundary conditions (10) in their dimensionless form read

$$\left.\begin{array}{llll} u=0\ , & w=0\,, & T=f=1 & at \quad r=r_i \\ u=\dfrac{\partial R}{\partial t}\ , & w=-\gamma_v\, K_n\left.\left(\dfrac{\partial w}{\partial r}\right)\right|_{r=R}\ , & T=f=0 & at \quad r=R \end{array}\right\}. \tag{19}$$

where

$R = \sqrt{r_o^{\,2} - \varepsilon^2 \sin^2\psi} - \varepsilon\cos\psi\,, \quad r_o = R_o + \phi\cos 2\pi(z-ct)\,.$

Here $R_o = 1/(1-r^*)$, $r_i = r^*/(1-r^*)$, $r^* = \dfrac{r_i}{R_o}$ is the radius ratio, and r^*, and $K_n = \lambda_m / L$ where K_n is Kundsen number.

3. Method of solution

The closed solution for the axial velocity $w(r,z)$ are given by

$$w(r,z) = -\frac{a_2}{a_1} + a_8\ J_0(i\sqrt{a_1}\,r) + a_9\,Y_0(-i\sqrt{a_1}\,r), \tag{20}$$

The homotopy perturbation method (HPM), is a series expansion method used in the solution of nonlinear ordinary and partial differential equations. The method employs a homotopy transform to generate a convergent series solution of differential equations. In view of the HPM [27-29], Eqs. (17) and (18) satisfy the following relations:

$$H(p,\theta) = L(\theta) - L(\theta_{10}) + p\,L(\theta_{10}) + p \Big/ \left(1+\frac{4}{3}Ra\right)\left(Br\left(1+\beta^{-1}\right)\left(\frac{\partial w}{\partial z}\right)^2 + N_b \Pr\left(\frac{\partial \theta}{\partial r}\frac{\partial f}{\partial r}\right) + N_t \Pr\left(\frac{\partial \theta}{\partial r}\right)^2\right), \tag{21}$$

$$H(p,f) = L(f) - L(f_{10}) + p\,L(f_{10}) + p\left(\frac{N_t}{N_b}\frac{\partial^2 \theta}{\partial r^2}\right), \tag{22}$$

with $L = \dfrac{\partial^2}{\partial r^2} + \dfrac{1}{r}\dfrac{\partial}{\partial r}$ as the linear operator, the initial approximations θ_{10} and f_{10} can be defined as

$$\theta_{10}(r,z) = f_{10}(r,z) = \ln\left(\frac{r}{R}\right) \Big/ \ln\left(\frac{r_i}{R}\right). \tag{23}$$

The basic assumption is that the solution of Eqs. (21) and (22) can be expanded as a power series in p

$$\theta(r,p) = \theta_0 + p\,\theta_1 + p^2\,\theta_2 + \ldots\ldots, \tag{24}$$

$$f(r,p) = f_0 + p\,f_1 + p^2\,f_2 + \ldots\ldots\,. \tag{25}$$

Da	*M*	β	ε	τ	***Nur***	***Sh***
0.01	**3**	**0.7**	**0.1**	**1.66146**	**0.500380**	**-0.0413883**
0.03	**3**	**0.7**	**0.1**	**2.56945**	**0.465635**	**0.108033**
0.03	**5**	**0.7**	**0.1**	**2.52113**	**0.467466**	**0.0974556**
0.05	**5**	**0.9**	**0.1**	**3.27771**	**0.44354**	**0.217413**
0.05	**3**	**0.9**	**-0.1**	**3.53477**	**1.68000**	**0.647790**
0.05	**10**	**0.9**	**-0.1**	**3.19185**	**1.66650**	**0.543476**
0.02	**10**	**0.9**	**-0.1**	**2.35479**	**1.66023**	**0.357319**
0.03	**10**	**0.9**	**-0.1**	**2.73227**	**1.65885**	**0.429574**
0.03	**10**	**0.8**	**-0.1**	**2.63637**	**1.66196**	**0.432834**

Table (1). Values of τ , *Nur* and *Sh* for various values of *Da, M* , β , and ε .

Pr	N_b	N_t	ε	***Nur***	***Sh***
1.5	**3.5**	**2.5**	**0.1**	**0.44354**	**0.217413**
2.5	**3.5**	**2.5**	**0.1**	**3.39631**	**0.707577**
2.5	**2.5**	**2.5**	**0.1**	**2.88382**	**1.25146**
3.5	**2.5**	**3.5**	**0.1**	**9.84313**	**3.15414**
3.5	**3.5**	**3.5**	**-0.1**	**10.9901**	**2.08812**
3.5	**2.5**	**3.5**	**-0.1**	**9.84313**	**3.15414**

1.5	**2.5**	**3.5**	**-0.1**	**1.18259**	**1.23269**
2.5	**2.5**	**3.5**	**-0.1**	**4.56347**	**2.19342**
2.5	**2.5**	**2.5**	**-0.1**	**-0.333592**	**-0.451928**

Table (2). Values of *Nur* and *Sh* for various values of *Pr*, N_b, N_t, and ε .

The solution of temperature and nanoparticle phenomenon (for p =1) are constructed as follows:

$$\theta(r,z) = \ln\left(\frac{r}{R}\right)/\ln\left(\frac{r_i}{R}\right) + \theta_1(r,z) + \left(\frac{N_t+N_b}{2304}\right)\Big[a_{22}\, r^2 \left(J_1^{\,2}(a_3 r) - J_0(a_3 r)\, J_2(a_3 r)\right)$$
$$+ a_{23}\, r^2 \left(Y_1^{\,2}(a_3 r) - Y_0(a_3 r) Y_2(a_3 r)\right) + \left(a_{24}+a_{25}\right) r^4 \ {}_1F_2\,(\frac{3}{2};3,3;-a_3^{\,2}\, r^2)$$
$$+ a_{26}\, r^4 \ {}_3F_4\,(\frac{3}{2},2,2;1,3,3,3;-a_3^{\,2}\, r^2) + a_{27}\, r^6 \Big(3\ {}_2F_3\,(2,\frac{5}{2};1,4,4;-a_3^{\,2}\, r^2) -$$
$$2\ {}_3F_4\,(\frac{5}{2},3,3;1,4,4,4;-a_3^{\,2}\, r^2)\Big) + \left(a_{26}+a_{28}\right) r^4 \ {}_4F_5\,(\frac{3}{2},2,2,2;1,3,3,3,3;-a_3^{\,2}\, r^2)$$
$$+ a_{29}\, r^4 \ {}_4F_5\,(\frac{5}{2},3,3,3;1,4,4,4,4;-a_3^{\,2}\, r^2) + a_{30} \ln r + a_{31} \left(\ln r\right)^2 + a_{32} \left(\ln r\right)^3 +$$
$$a_{28}\, r^4 \ {}_3F_4\,(\frac{3}{2},2,2;1,3,3,3;-a_3^{\,2}\, r^2) + a_{33}\, r^2\, G_{46}^{5}\left(a_3\, r, \frac{1}{2}\middle|\begin{matrix} -\frac{1}{2},0,0,\frac{1}{2} \\ -1,-1,-1,1,1,-\frac{1}{2} \end{matrix}\right) +$$
$$a_{34}\, r^3 \left[G_{57}^{6}\left(a_3\, r, \frac{1}{2}\middle|\begin{matrix} -1,-\frac{1}{2},-\frac{1}{2},0,\frac{1}{2} \\ -\frac{3}{2},-\frac{3}{2},-\frac{3}{2},-\frac{3}{2},\frac{3}{2},\frac{3}{2},-1 \end{matrix}\right) + G_{46}^{32}\left(a_3\, r, \frac{1}{2}\middle|\begin{matrix} -\frac{1}{2},-\frac{1}{2},0,0 \\ -\frac{1}{2},-\frac{1}{2},-\frac{1}{2},-\frac{3}{2},-\frac{3}{2},0 \end{matrix}\right)\right] +$$
$$a_{35}\, r^2\, G_{57}^{6}\left(a_3\, r, \frac{1}{2}\middle|\begin{matrix} -\frac{1}{2},0,0,0,\frac{1}{2} \\ -1,-1,-1,-1,1,1,-\frac{1}{2} \end{matrix}\right) + a_{36}\, r^3\, G_{46}^{14}\left(a_3\, r, \frac{1}{2}\middle|\begin{matrix} -\frac{1}{2},-\frac{1}{2},0,\frac{1}{2} \\ \frac{3}{2},-\frac{3}{2},-\frac{3}{2},-\frac{3}{2},-\frac{3}{2},\frac{3}{2} \end{matrix}\right) \qquad , \quad (26)$$
$$+ a_{37}\, r^2\, G_{57}^{24}\left(a_3\, r, \frac{1}{2}\middle|\begin{matrix} 0,0,0,\frac{1}{2},-\frac{1}{2} \\ 0,1,-1,-1,-1,-1,-\frac{1}{2} \end{matrix}\right)$$

$$f(r,z) = \left(1 - \frac{N_t}{N_b}\right)\left(\ln\left(\frac{r}{R}\right)/\ln\left(\frac{r_i}{R}\right)\right) - \frac{N_t}{N_b}\,\theta_1(r,z) + a_{14} \ln(r) + a_{15}, \qquad (27)$$

$$\theta_1(r,z) = a_{38} - \left(\frac{N_t+N_b}{4\sqrt{\pi}}\right)\Big[a_{16}\, r^4 \ {}_3F_4\,(\frac{3}{2},2,2;1,3,3,3;-a_3^{\,2}\, r^2) + a_{17}\, r^2 \left(J_1^{\,2}(a_3 r) - \right.$$
$$\left. J_0(a_3 r)\, J_2(a_3 r)\right) + a_{18}\, r^2 \left(Y_1^{\,2}(a_3 r) - Y_0(a_3 r) Y_2(a_3 r)\right) - 4a_{20} \ln r +$$
$$2a_{19} \left(\ln r\right)^2 + 2\, a_{18}\, G_{46}^{5}\left(a_3\, r, \frac{1}{2}\middle|\begin{matrix} -\frac{1}{2},0,0,\frac{1}{2} \\ -1,-1,-1,1,1,-\frac{1}{2} \end{matrix}\right) + 2\, a_{21}\, G_{46}^{23}\left(a_3\, r, \frac{1}{2}\middle|\begin{matrix} 0,0,\frac{1}{2},-\frac{1}{2} \\ 0,1,-1,-1,-1,-\frac{1}{2} \end{matrix}\right)\Big], \qquad (28)$$

The mathematical formulas of the constants $a_1 - a_{38}$ are not included here. However, they are available upon request from the author.

Now, the reduced Nusselt number *Nur* and Sherwood number *Sh* at the outer annulus are defined, respectively, by

$$Nur = \left.\frac{\partial \theta}{\partial r}\right|_{r=r_o}, \qquad Sh = \left.\frac{\partial f}{\partial r}\right|_{r=r_o}. \tag{29}$$

6. Numerical results and discussion

In order to get an insight into the physical situations of the problem, we have computed numerical values of the axial velocity, temperature and nanoparticles phenomena for different values of various parameters occurring in the problem.

The effects of physical parameters on the temperature distribution are indicated through figures (1-4). Figs. (1) and (2) show the effect of Brinkman number B_r on the temperature profiles with the radial coordinate r in the cases when the eccentricity ε is positive and negative, respectively. It is observed from Fig. (1) that as B_r increases the temperature increases, when $\varepsilon > 0$, it is also noted that the difference of the temperature for different values of B_r becomes greater with increasing the radial coordinate and reaches maximum value after which it decreases. Fig. (2) shows that, for $\varepsilon < 0$, the curves are found to be similar to the curves in fig. (1), with the only difference that the temperature decreases as B_r increases near the outer annuli, namely when $r \epsilon\ [1.2, 2.5]$. The effects of D_a, N_b and β on the temperature T are found to be exactly similar to the effect of B_r given in Fig. (2a, b). Similar result to that shown in Fig. (1) can be obtained if *Br* is replaced by *Da* with the only difference that the obtained curves are very close to those obtained in Fig. (2). Fig. (3) shows the variation of T with the radial coordinate r for various values of radiation parameter *Ra* when the eccentricity $\varepsilon > 0$. It is found that the temperature T decrease with the increase of *Ra*. also, it is indicated that T decreases with r till a maximum value (represents the maximum value of T), value after which it decreases and the obtained curves coincide near the outer annuli. Figure (4) illustrates the effect of the thermophoresis parameter N_t on the temperature distribution T when the eccentricity ε is negative. It is found that the temperature T increases by increasing N_t in the intervals $r \in [0.5,\ 0.9] \cup [1.3,\ 2.5]$; otherwise it decreases by increasing N_t. So, the behavior of T in the interval $r \in\ [0.9, 1.3]$, is an inversed manner of its behavior in the other intervals. In this case, for each value of N_t, there are maximum values of T hold at r =0.7, 1.8. Similar result to that shown in Fig. (4) can be obtained if N_t is replaced by Da with the only difference that the obtained curves are very close to those obtained in Fig. (4).

The nanoparticles phenomena f for different values of Brownian motion parameter N_b when $\varepsilon > 0$ is shown in Fig. (5), and it is shown that the nanoparticles phenomena f increases by increasing N_b in the range of r shown in the figure, namely in the interval $r \in [0.5, 1.1]$, otherwise it decreases as with the increase of N_b. Also for small values of N_b, the nanoparticles phenomena decreases with r, till a minimum value (at a finite value of $r : r = r_0$) after which it increases. Also, it is clear that the minimum of f decreases by increasing N_b and this also occurs at another value $r < r_0$. Fig. (6) reveals the influence of Darcy number Da on the nanoparticles phenomena f when the eccentricity ε is negative. It is indicated that the nanoparticles phenomena f decreases with the increasing of Da in the interval $r \in [0.5, \ 0.9]$, whereas it increases as Da increases when $r \in [0.9, \ 1.5]$. It is also noted that f is always positive, and it decreases as r increases, and reaches minimum value (at a finite value of $r : r = r_0$) after which it increases and reaches maximum value at another value of r. the effects of the other parameters are found to be similar to them; these figures are excluded here to avoid any kind of repetition.

Figs. (7) and (8) illustrate the change of the axial velocity w versus the radial coordinate r with several values of the upper limit apparent viscosity coefficient β and magnetic parameter M, respectively, when the eccentricity $\varepsilon > 0$. It is seen, from Figs. (7) and (8), that the axial velocity increases with the increase of β, whereas it decreases as M increases, respectively. It is also noted that the difference of the axial velocity for different values of β and M becomes greater with increasing the radial coordinate and reaches maximum value after which it decreases. Note that the maximum value of w increases by increasing β and M and this also occurs at another value $r > r_0$. The effects of Da on the axial velocity w are found to be exactly similar to the effect of β given in Fig. (7).

Tables. (1), (2) and (3), presents numerical results for the quantities τ, Nur and Sh which are representative of the skin friction, the reduced Nusselt number and Sherwood number respectively, for various values of all parameters when the eccentricity ε is positive and negative. It is clear from table (1) that an increase in Darcy number Da and the upper limit apparent viscosity coefficient β gives an increase in the values of quantities τ and Sh but decreases the dimensionless quantity Nur. Also, an increase in the magnetic parameter M gives an opposite behavior to both Da and β. The values of both Nur and Sh for various values of Prandtl number Pr, the thermophoresis parameter N_t, Brownian motion parameter

N_b are presented in table (3). It is noted that the dimensionless quantities Nur and Sh increase as Pr and N_t increase. But an increase in N_b gives an increase in the values of dimensionless quantity Nur but decreasing in the dimensionless quantity Sh.

7. Conclusion

MHD peristaltic mechanism with heat transfer of an incompressible non-Newtonian nanofluid through a porous media in eccentric annuli with slip velocity condition at the wall, and under the consideration of long wavelength and low-Reynolds number has been studied. The expressions of the axial velocity is obtained in a closed form, while the solutions for energy and nanoparticles equations are obtained by using homotopy perturbation method. Also, the reduced Nusselt number and Sherwood number at the outer annulus are obtained and tabulated for positive and negative eccentricity. The results of this problem are of great importance in many industrial heating or cooling equipments. The nanoparticles are typically made up of metals, oxides, and carbides or carbon nanotubes. The main findings from the current study can be summarized as follows:

(1) The nanoparticles phenomena f decreases with increasing each of β, N_t, Da, Br and Pr. It increases near the outer annuli in case of Da and Br, whereas it increases by increasing values of M, N_b and Ra.

(2) The nanoparticles phenomena f is always positive, and there is an inverse relation between f and the radial coordinate r.

(3) The temperature θ has an opposite behavior compared to nanoparticles behavior except that it increases or (decreases) with the increase of both N_b and Pr.

(4) The temperature θ for different values of all parameters of the problem and for positive eccentricity ε, increases by increasing the radial coordinate r and reaches maximum value (at a finite value of $r : r = r_0$) after which it decreases.

(5) Oscillatory behavior is observed in all figures for the temperature T when the eccentricity ε is negative.

(6) The axial velocity w for both positive and negative values of eccentricity ε, increases with the increase each of β and Da, while it decreases as M increase.

(7) By increasing the radial coordinate r, the axial velocity w for different values of β, Da, γ and M becomes greater and larger and reaches maximum value, after which it decreases.

(8) The skin-friction distribution τ_ω decreases by increasing M, while it increases as Da and β increase. This occurs for positive and negative eccentricity.

(9) For positive values of eccentricity ε, Nusselt number *Nu* increases, by increasing each of M, Pr, N_b and N_t whilst it decreases as Da and β increases.

(10) Sherwood number *Sh* has an opposite behavior compared to Nusselt number *Nu*.

References

1) Wang, X.Q., Mujumdar, A. S., Heat Transfer Characteristics of Nanofluids: A Review, Int. J. Thermal Sci. 46 (2007), pp. 1-19
2) Nadeem, S., Haq, R. U., MHD Boundary Layer Flow Of A Nanofluid Passed Through A Porous Shrinking Sheet With Thermal Radiation, J. Aerosp. Eng. 28 (2015), 04014061.
3) Mustafa, M., Hayat, T., Pop, I., Asghar, S., Obaidat, S., Stagnation-Point Flow of A Nanofluid Towards A Stretching Sheet, Int. J. Heat Mass Transfer, 54 (2011), pp. 5588–5594
4) Ho, C. J., Chen, M. W., Li, Z. W., Numerical Simulation of Natural Convection of Nanofluid in a Square Enclosure: Effect Due To Uncertainties of viscosity And Thermal Conductivity, Int. J. Heat Mass Transfer, 51 (2008), pp. 4506–4516
5) Santra, A. K., Sen, S., Chakraborty, N., Study of Heat Transfer Augmentation In A Differentially Heated Square Cavity Using Copper–Water Nanofluid, Int. J. Therm. Sci. 47 (2008), pp. 1113–1122
6) Mahmoudi, A. H., Shahi, M., Talebi, F., Effect of Inlet And Outlet Location On The Mixed Convective Cooling Inside The Ventilated Cavity Subjected To An External Nanofluid, Int. Commun. Heat Mass Transfer, 37 (2010), pp. 1158–1173
7) Mahmoudi, A. H., Shahi, M., Shahedin, A.M., Hemati, N., Numerical Modeling of Natural Convection In An Open Cavity With Two Vertical Thin Heat Sources Subjected To A Nanofluid, Int. Commun. Heat Mass Transfer, 38 (2011), pp. 110–118
8) Abu-Nada, E., Effects of Variable Viscosity And Thermal Conductivity of Al_2O_3–Water Nanofluid On Heat Transfer Enhancement In Natural Convection, Int. J. Heat Fluid Flow 30 (2009), pp. 679–690
9) Khaled, A. R. A., Vafai, K., Heat Transfer Enhancement Through Control of Thermal Dispersion Effects, Int. J. Heat Mass Transfer, 48 (2005), pp. 2172–2185
10) Kuznetsov, A. V., Nield, D. A., Natural Convective Boundary-Layer Flow of A Nanofluid Past A Vertical Plate, Int. J. Thermal Sci. 49 (2010), pp. 243–247
11) Choi, S. U. S., Enhancing Thermal Conductivity of Fluids With Nanoparticles, ASME Fluids Eng. Div. 231 (1995), pp. 99–105

12) Chen, R. X., Liu, F. J., J. He, H., Fan, J., Silk Cocoon: "Emperor's New Clothes" for Pupa: Fractal Nano-Hydrodynamical Approach, J. Nano Res. 22 (2013), pp. 65-70

13) Eldabe, N. T., Abou-zeid, M. Y., Magnetohydrodynamic Peristaltic Flow With Heat And Mass Transfer of Micropolar Biviscosity Fluid Through A Porous Medium Between Two Co-Axial Tubes, Arab J. Sci. Eng. 39 (2014), pp. 5045–5062

14) Mustafa, M., Hina, S., Hayat, T., Alsaedi, A., Influence of Wall Properties On The Peristaltic flow of A Nanofluid: Analytic And Numerical Solutions, Int. J. Heat Mass Transfer 55 (2012), pp. 4871–4877

15) Akbar, N. S., Nadeem, S., Endoscopic Effects On Peristaltic Flow of A Nanofluid, Commun. Theor. Phys. 56 (2011), pp. 761–768

16) Akbar, N. S., Nadeem, S., Hayat, T., Hendi, A. A., PeristalticFlow of A Nanofluid With Slip Effects, Meccanica, 47 (2012), pp. 1283-1294

17) Eldabe, N. T., Abou-zeid, M. Y., The Wall Properties Effect On Peristaltic Transport of Micropolar Non-Newtonian Fluid With Heat And Mass Transfer. Math. Prob. Eng. (2010), Article ID 898062, 40 pages.

18) Akbar, N. S., Nadeem, S., Hayat, T., Hendi, A. A., Peristaltic Flow of A Nanofluid In A Non-Uniform Tube, Heat Mass Transfer/Waerme-und Stoffuebertragung 48 (2012), pp. 451–459

19) Akbar, N. S., Nadeem, S., Peristaltic Flow of A Phan–Thien–Tanner Nanofluid In A Diverging Tube, Heat Transfer, 41 (2012), pp. 10–22

20) Ebaid, A., Aly, E. H., Exact Analytical Solution of The Peristaltic Nanofluids Flow In An Asymmetric Channel With Flexible Walls And Slip Condition: Application To The Cancer Treatment, Comput. Math. Meth. Med. (2013), Article ID 825376, 8 pages.

21) Ebaid, A., Remarks On The Homotopy Perturbation Method For The Peristaltic Flow of Jeffrey Fluid With Nano-Particles In An Asymmetric Channel, Comput. Math. Appl. 68 (2014), pp. 77–85

22) Nelson, E. B., Well Cementing, Elseivier, Amsterdam, New York, USA, 1990

23) Walton, I. C., Bittleston, S. H., The Flow of A Bingham Plastic Fluid In A Narrow Eccentric Annulus, J. Fluid Mech. 222 (1991), pp. 39-60

24) Ahmed, M. E. S., Attia, H. A., Magnetohydrodynamic Flow And Heat Transfer of A Non-Newtonian Fluid In An Eccentric Annulus, Can. J. Phys. 76 (1998), pp. 391-401

25) El-Sayed, M. F., Eldabe, N. T., Ghaly, A. Y., Sayed, H. M., Magnetothermodynamic Peristaltic Flow of Bingham Non-Newtonian Fluid in Eccentric Annuli With Slip Velocity and Temperature Jump Conditions, J. Mechanics, 29 (2013), pp. 493–506

26) Rohsenow, W. M., Hartnett, J. P., Cho, Y. I., Handbook of Heat Transfer, McGraw-Hill, New York, USA, 1998

27) Davood, D. G., Zaman, Z. G., Hosain, D. G., Determination of temperature distribution for annular fins with temperature dependent thermal conductivity by HPM, Thermal Sci. 15 (2011), pp. S111–S115

28) He, J. H., Homotopy Perturbation Technique, Comput. Methods Appl. Mech. Eng. 178 (1999), pp. 257-262

29) Rajeev, Homotopy perturbation method for a Stefan problem with variable latent heat, Thermal Sci. 18 (2014), pp. 391–398

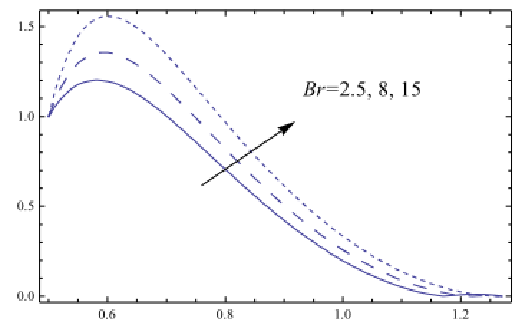

Fig. (1)

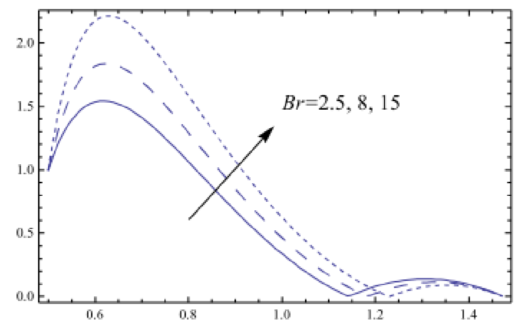

Fig. (2)

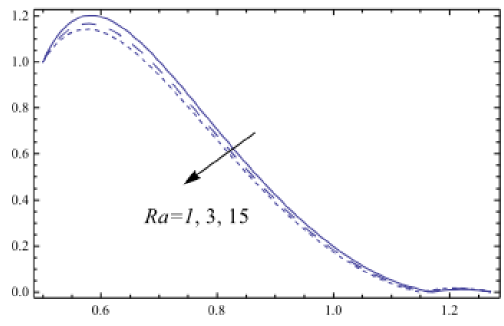

Fig. (3)

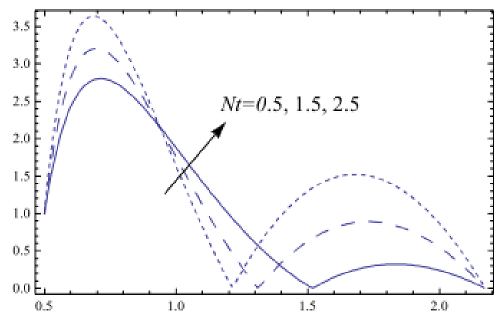

Fig. (4)

Fig. (1). The temperature profiles are plotted versus r for different values of Br for a system have the particulars ε=0.1 β=0.9, Da=0.05, M=3, Ra=1, Pr=1.5, Nb=3.5, Nt=2.5, z=1, r^*=0.33, dP/dz=5, γ_v=0.2, K_n=0.05, ψ=0, t=0.3, and ϕ=0.41 .

Fig. (2). The temperature profiles are plotted versus r for different values of Br for a system have the particulars $\varepsilon=-0.1$ $\beta=0.9$, Da=0.05, M=3, Ra=1, Pr=1.5, Nb=3.5, Nt=2.5, z=1, $r^*=0.33$, dP/dz=5, $\gamma_v=0.2$, $K_n=0.05$, $\psi=0$, t=0.3, and $\phi=0.41$.

Fig. (3). The temperature profiles are plotted versus r for different values of Ra for a system have the particulars $\varepsilon=0.1$ $\beta=0.9$, Da=0.05, M=3, Br=2.5, Pr=1.5, Nb=3.5, Nt=2.5, z=1, $r^*=0.33$, dP/dz=5, $\gamma_v=0.2$, $K_n=0.05$, $\psi=0$, t=0.3, and $\phi=0.41$.

Fig. (4). The temperature profiles are plotted versus r for different values of Nt for a system have the particulars $\varepsilon=-0.1$ $\beta=0.9$, Da=0.05, M=3, Br=2.5, Ra=1, Pr=1.5, Nb=3.5, z=1, $r^*=0.33$, dP/dz=5, $\gamma_v=0.2$, $K_n=0.05$, $\psi=0$, t=0.3, and $\phi=0.41$.

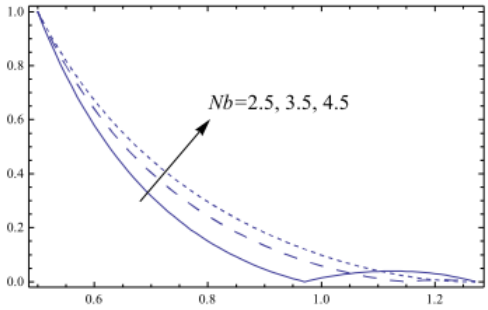

Fig. (5)

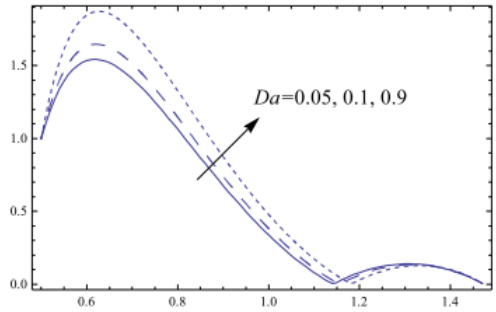

Fig. (6)

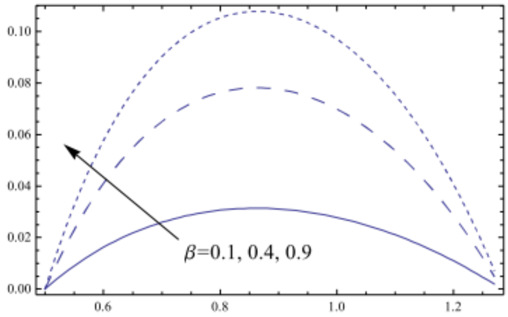

Fig. (7)

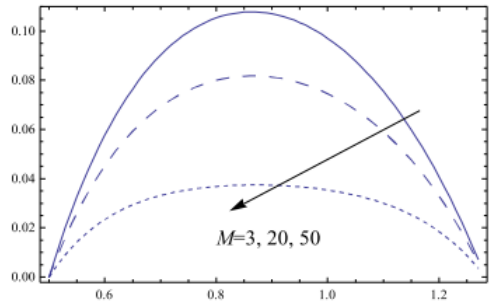

Fig. (8)

Fig. (5). The nanoparticles profiles are plotted versus r for different values of Nb for a system have the particulars $\varepsilon=0.1$ $\beta=0.9$, Da=0.05, M=3, Br=2.5, Ra=1, Pr=1.5, Nt=2.5, z=1, $r^*=0.33$, dP/dz=5, $\gamma_v=0.2$, $K_n=0.05$, $\psi=0$, t=0.3, and $\phi=0.41$.

Fig. (6). The nanoparticles profiles are plotted versus r for different values of Da for a system have the particulars $\varepsilon=-0.1$ $\beta=0.9$, M=3, Br=2.5, Ra=1, Pr=1.5, Nb=3.5, Nt=2.5, z=1, $r^*=0.33$, dP/dz=5, $\gamma_v=0.2$, $K_n=0.05$, $\psi=0$, t=0.3, and $\phi=0.41$.

Fig. (7). The axial velocity profiles are plotted versus r for different values of β for a system have the particulars $\varepsilon=0.1$, Da=0.05, M=3, Br=2.5, Ra=1, Pr=1.5, Nb=3.5, Nt=2.5, z=1, $r^*=0.33$, dP/dz=5, $\gamma_v=0.2$, $K_n=0.05$, $\psi=0$, t=0.3, and $\phi=0.41$.

Fig. (8). The axial velocity profiles are plotted versus r for different values of M for a system have the particulars ε=0.1 β=0.9, Da=0.05, Br=2.5, Ra=1, Pr=1.5, Nb=3.5, Nt=2.5, z=1, r^*=0.33, dP/dz=5, γ_v=0.2, K_n=0.05, ψ=0, t=0.3, and ϕ=0.41 .